

Efficiency Measurements and Installation of a New Grating for the OSIRIS Spectrograph at Keck Observatory

Etsuko Mieda^{1,2,a}, Shelley A. Wright^{1,2}, James E. Larkin³, James R. Graham^{2,5}, Sean M. Adkins⁴, James E. Lyke⁴, Randy D. Campbell⁴, Jérôme Maire², Tuan Do², and Jacob Gordon^{1,2}

¹*Department of Astronomy & Astrophysics, University of Toronto, ON, CANADA, M5S 3H4*

²*Dunlap Institute for Astronomy & Astrophysics, University of Toronto, ON, CANADA, M5S 3H4*

³*Division of Astronomy and Astrophysics, University of California, Los Angeles, CA, USA, 90095*

⁴*W. M. Keck Observatory, HI, USA, 96743*

⁵*Astronomy Department, University of California, Berkeley, CA, USA, 94720*

ABSTRACT

OSIRIS is a near-infrared integral field spectrograph operating behind the adaptive optics system at W. M. Keck Observatory. While OSIRIS has been a scientifically productive instrument to date, its sensitivity has been limited by a grating efficiency that is less than half of what was expected. The spatially averaged efficiency of the old grating, weighted by error, is measured to be 39.5 ± 0.8 % at $\lambda = 1.310$ μm , with large field dependent variation of 11.7 % due to efficiency variation across the grating surface. Working with a new vendor, we developed a more efficient and uniform grating with a weighted average efficiency at $\lambda = 1.310$ μm of 78.0 ± 1.6 %, with field variation of only 2.2 %. This is close to double the average efficiency and five times less variation across the field. The new grating was installed in December 2012, and on-sky OSIRIS throughput shows an average factor of 1.83 improvement in sensitivity between 1 and 2.4 microns. We present the development history, testing, and implementation of this new near-infrared grating for OSIRIS and report the comparison with the predecessors. The higher sensitivities are already having a large impact on scientific studies with OSIRIS.

Subject headings: Astronomical Instrumentation, Astronomical Techniques

1. Introduction

In the last decade, the combination of a near-infrared integral field spectrograph (IFS) and adaptive optics (AO) has proven to be crucial in a range of astronomical studies from our solar system to galaxies in the early universe. Some example observations include the sulphur dioxide distribution on one of the Galilean moons, Io (Laver & de Pater 2009), morphology of novae ejecta (Lyke & Campbell 2009), the atmosphere of an extrasolar gas giant planets (e.g. Barman et al. 2011; Konopacky et al. 2013), the crowded stellar fields of the Galactic Center (e.g.

Trippe et al. 2008; Do et al. 2009, 2013), AGN (e.g. Davies et al. 2007; McConnell et al. 2011; Contini et al. 2012), and high redshift galaxies (e.g. Förster Schreiber et al. 2006; Law et al. 2009; Wright et al. 2009; Wisnioski et al. 2011). IFSs are also aimed to be the first eight instruments for the next generation of extremely large telescopes, such as IRIS on TMT (Larkin et al. 2010), HARMONI on E-ELT (Thatte 2010), and GMTIFS on GMT (McGregor et al. 2012).

OSIRIS (OH-Suppressing Infrared Imaging Spectrograph) (Larkin et al. 2003, 2006), a moderate spectral resolution ($R \sim 3800$) diffraction limited IFS for the AO system at W. M. Keck Observatory, is one of a handful of IFS instru-

^amieda@astro.utoronto.ca

ments in use with AO systems worldwide today. It was the first diffraction limited IFS instrument to use a lenslet array as the sampling element on the sky and has plate scales ranging from 0.02" to 0.1" per spaxel¹. OSIRIS' optics and lenslet array produce low non-common path error (<30 nm rms), a factor of approximately three times less than any other IFS, preserving the diffraction limited point spread function of the Keck AO system (Wizinowich et al. 2006).

OSIRIS was designed with a single fixed diffraction grating to ensure spectral stability and make data reduction possible with very dense spectral packing on the detector (only two pixel spacing between spectra). The grating is used in multiple orders (m) to cover traditional near-infrared wavebands: K ($\lambda_{cen} = 2.2 \mu\text{m}$) is sampled in $m = -3$, H ($\lambda_{cen} = 1.6 \mu\text{m}$) in $m = -4$, J ($\lambda_{cen} = 1.3 \mu\text{m}$) in $m = -5$, and Z ($\lambda_{cen} = 1.1 \mu\text{m}$) in $m = -6$.

While OSIRIS has been a productive instrument to date, its performance has been limited by sensitivity, which is approximately 50 % lower than its design prediction, particularly at shorter wavelengths (Z and J bands). Through our team's investigation, this performance limitation has been determined to be due to the quality of the spectrograph's diffraction grating. Since 2009 our team actively pursued acquiring a new grating for the OSIRIS spectrograph. In 2011, we began to work with the Bach Research Corporation, Boulder, CO, to fabricate a new, more efficient grating for OSIRIS. Our goal was to improve the grating performance sufficiently to double the signal to noise ratio for detector limited observations.

In this paper, we describe our acquisition and testing of a new grating. In §2, we summarize the history of the OSIRIS spectrograph grating. In §3 we describe the laboratory setup used to measure the grating efficiency and the results of those measurements. In §4, we report on the December 2012 installation of the new grating. In §5, we discuss the on-sky performance of OSIRIS with the new grating. For interested in equipment characterization, Appendix A and B describe camera and laser diode characterization processes in detail. For the user of OSIRIS or other IFS instruments, we introduce the OSIRIS data reduction pipeline and the modifications made after installation of the new

grating in Appendix D.

2. History of OSIRIS Grating

The OSIRIS spectrograph grating is a unique and unusual single fixed diffraction grating that has a coarse ruling of 27.93 grooves per mm at a shallow blaze angle of 5.76° . The specifications of the grating are listed in Table 1.

The grating design was done by Richardson Gratings, Rochester, NY, in collaboration with SSG Precision Optonics, Inc., Wilmington, MA, the designers and fabricators of the OSIRIS collimator and camera three-mirror anastigmats.

Over the time OSIRIS has been in service at Keck Observatory, we have installed three different gratings. They are summarized in Table 2.

Originally, SSG manufactured two large aluminum grating blanks and provided these to Richardson Gratings for ruling. However, this first option for ruling was abandoned by them due to the large amount of tool pressure that would be required. A new vendor, Diffraction Products, Inc., Woodstock, IL, then agreed to take on the challenge of ruling this very coarse grating directly into a pure gold coating placed on the SSG aluminum blank. The resulting grating is identified as G1 in Table 2.

During laboratory testing of OSIRIS in October 2004, it was determined that G1 had a slightly varying, incorrect (6.2° instead of 5.76°) blaze angle. At high order, this puts the majority of the light into the wrong order and off the field of the detector. Efficiencies in the Z and J band were below 20% and even in the K -band was below 30%. Due to time constraints, OSIRIS was shipped to the telescope with this imperfect grating while a replacement was ordered. Diffraction products significantly improved their process and a replacement grating with the correct blaze angle (called G2) was installed in OSIRIS in June 2005.

Figure 1 is a photograph of diffraction spots on a wall by G1 (left) and G2 (right) at the Keck Observatory in June 2005. The left image shows scattered light between the different orders due to incomplete ruling. This shows the improvement of the grating quality visually. The throughput measurement at the time of the servicing mission showed a gain of a factor of three to four in J band

¹Spectrum of each spatial element.

TABLE 1
OSIRIS GRATING SPECIFICATION

| Parameter | Value |
|----------------------|------------------------------------|
| Size | 275 × 220 × 50 mm |
| Line Spacing | 27.93 lines/mm |
| Blaze Angle | 5.76° |
| Clear Aperture | 205 × 230 mm (min.) |
| Surface Irregularity | 150 nm RMS |
| Surface | Gold coating on aluminum substrate |

TABLE 2
SUMMARY OF ALL THREE OSIRIS GRATINGS

| Grating | Manufacturer | Service Duration | J Efficiency |
|---------|----------------------------|---------------------|----------------|
| G1 | Diffraction Products, Inc. | Feb 2005 - May 2005 | ~ 15 % |
| G2 | Diffraction Products, Inc. | Jun 2005 - Dec 2012 | 39.5 % |
| G3 | Bach Research Corporation | Jan 2013 - present | 78.0 % |

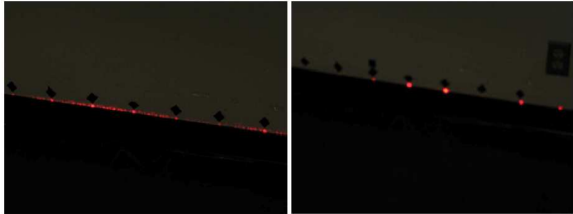


Fig. 1.— A photograph of diffraction spots at the Keck Observatory in June 2005. It shows a HeNe laser at 632.8 nm being diffracted by G1 (left) and G2 (right). The locations of diffraction spots were marked with electrical tape. Note that G1 produces dramatic light loss between the orders compared to G2.

with a smaller gain at longer wavelengths.

Unfortunately, even with G2, the throughput was still ~ 50 % of what was expected. This was later confirmed by our team during an October 2009 servicing mission. G2 was removed from OSIRIS, and its efficiency was measured at Keck Observatory using a 1.310 μm laser (close to 5th order expected blaze wavelength) and an infrared camera. The resulting absolute efficiency measurements are shown in Figure 2. This was

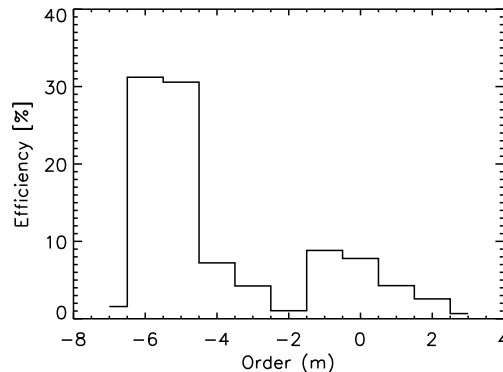


Fig. 2.— Measurements of absolute efficiency by order for G2 at the Keck summit in 2011. The blaze wavelength is 6.5 μm , so the 5th order should have the maximum power at ~60 to 70 %.

also verified with atomic force microscope (AFM) scans of G2. An AFM scan of one of the grating facets is shown in Figure 3. The grating facet shows a flat spot at the edge of the ruling, and the profile on the primary facet has at least two distinct angles. The effect of the curved profile on the steep side of the profile is to distribute some of

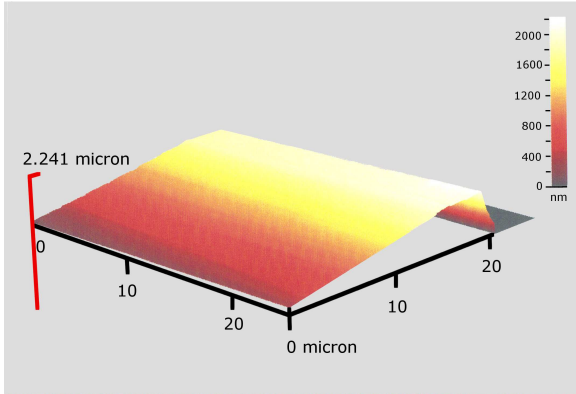


Fig. 3.— AFM scan of one of the facets of G2 made by Diffraction Products, illustrating the curved profile on the facet, which decreases the overall sensitivity in each order.

the energy from the expected order into adjacent orders. The expected effect of the flat spot in the facets is that it causes some of the light to be scattered across all of the orders. We do not know if the same facet profile occurs throughout the grating, but both of these effects are clearly visible in our efficiency plot in Figure 2. Most likely, G2 has generally poor quality groove shapes like Figure 3. If all of the energy between orders -5 and -6 in Figure 2 were concentrated in the expected order ($m = -5$), the efficiency at $1.310 \mu\text{m}$ would be $> 60 \%$ as expected from the specifications.

At this point, the OSIRIS team began a search for a new vendor to manufacture a better quality grating. Bach Research Corporation, formed by the founding members of the Hyperfine company, began making custom astronomical gratings, and we selected them in 2011 to begin the process of ruling a new grating on the original SSG blank.

The first and second OSIRIS gratings were directly ruled into a gold coating applied to a machined one piece aluminum grating substrate and grating mount. Rather than directly ruling into the grating substrate, Bach Research suggested that we replicate the grating onto the aluminum substrate and then coat the replica with gold. The one piece machined aluminum grating mount and substrate is an expensive component to machine, so we made use of the spare grating mount used during the first attempt of the grating by Diffraction Products. To produce the new grating, Bach

Research removed the coating from G1 mount and re-polished it. This provided a new surface to apply a new ruling using a replication process. The fabrication was performed in two steps by Bach Research Corporation:

- (1) A new master grating was ruled onto a Zerodur substrate (a glass-ceramic composite material produced by Schott AG).
- (2) The new master was used for replication of the grating on a new coating on the spare substrate (called G3).

As part of the contract discussions for the new grating, Bach Research made a demonstration test ruling on a small $5 \text{ mm} \times 100 \text{ mm}$ long substrate. A comparison of a diffraction of a HeNe laser at 632.8 nm with both this substrate and G1, taken at Bach Research is shown in Figure 4. The left

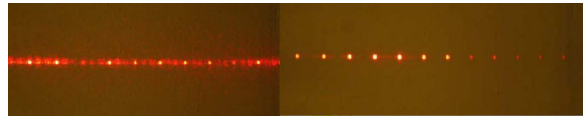


Fig. 4.— Diffraction of HeNe laser at 632.8 nm using G1 (left) and the test ruling made by Bach Research (right) compared at Bach Research.

image is the diffraction spots produced by G1 and the right image is by the test ruling. The light diffracted by the test ruling is well concentrated in spots while G1 smears the light in the direction of dispersion.

One of the important challenges encountered in the manufacture of the previous gratings was that the grating maker could only evaluate the grating performance using a simple set up involving a HeNe laser with visual evaluation of the resulting dispersion and relative intensities in each order. The method used did not predict the grating's eventual performance at infrared wavelengths. Before installation of G3 we acquired an infrared laser source ($1.310 \mu\text{m}$) and infrared camera and created a set-up that allowed measurement of the grating efficiency in a reliable fashion. This allowed us to evaluate the test ruling as well as the final grating before it was installed in OSIRIS.

3. Grating Efficiency Measurement

To investigate the grating performance in a more robust manner, we measure the direct efficiency of the grating at $\lambda = 1.310 \mu\text{m}$, which corresponds to a wavelength in the *J* band. In this section, we describe the measurement equipment, measurement setup, procedure, and discuss the measurement results.

3.1. Measurement Equipment and Stability

For the grating efficiency measurements in infrared, we used an InGaAs camera (Raptor Photonics OWL SW 1.7 CL-320) and a $1.310 \mu\text{m}$ laser diode coupled to a SMF-28 fiber (a single mode fiber with a core diameter of $8.2 \mu\text{m}$ operating at $1.310 \mu\text{m}$ to $1.625 \mu\text{m}$). The linearity of the camera and the stability of the laser are discussed in Appendices A and B. Some preliminary tests were done on a $5 \times 100 \text{ mm}$ test ruling that Bach Research fabricated in early 2012 before G3 manufacture. In summary, we find that 10 data number (DN) noise level in the camera, a 0.3 % fluctuation due to a 10°C camera temperature change, and a 3.5 % fluctuation in laser diode intensity over a one hour period.

3.2. Measurement Setup and Procedure

To measure the efficiency of the grating at the same configuration as in OSIRIS, we set up an optical path on an optical bench, where the angle of incidence (α) is $\alpha = -30.2^\circ$, and the angle of diffraction (β) for $m = -5$ at $1.310 \mu\text{m}$ is $\beta = 18.4^\circ$. We define the sign conventions and orientation for the OSIRIS grating used throughout our measurements in Figure 5. In our setup, the incident angle is accurate within 1° , which is theoretically a $<1\%$ change in $m = -5$ efficiency at $1.310 \mu\text{m}$ (Figure 6) using our Rigorous Coupled-Wave Analysis (RCWA) (Moharam & Gaylord 1981) code. RCWA is a semi-analytic computational method used to solve Maxwell’s equations. Our code uses this method to calculate the portion of light being diffracted into different orders by a diffraction grating for the given grating specification, Table 1, and the incident angle.

A $1.310 \mu\text{m}$ laser diode that is coupled to a SMF-28 fiber is connected to an attenuator and a collimator. The collimated laser beam goes

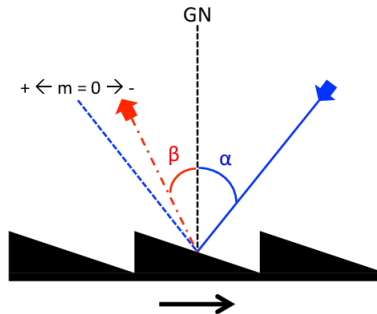


Fig. 5.— Orientation of OSIRIS grating blaze direction (black arrow), incident angle α (blue and negative), and outgoing angle β (red, dot-dash line and positive). Negative orders are defined to be in the direction towards the grating normal (GN) from $m = 0$ (pure reflection).

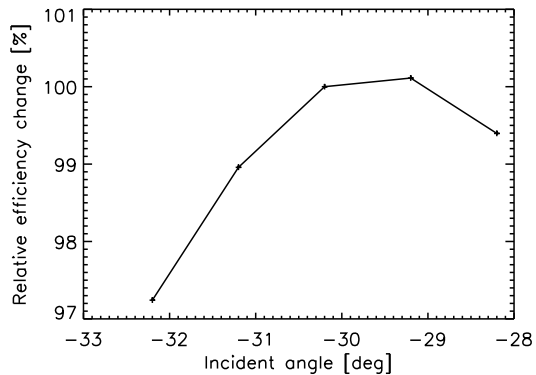


Fig. 6.— RCWA analysis prediction of the theoretical $m = -5$ efficiency change at $\lambda = 1.310 \mu\text{m}$ due to the incident angle change. With a 1° change in the incident angle, the change in efficiency is less than 1%.

through two neutral density (ND) filters and hits the grating surface, where it is diffracted into constituent orders. An achromatic lens pair focuses the beam on the InGaAs camera, which sits on a dovetail optical rail system. The beam’s full-width-half-maximum at $m = -5$ is about 1.7 mm on the camera. The schematic of the configuration is shown in Figure 7, and a photo of the setup is

on Figure 8. An aluminum baffle box resides over

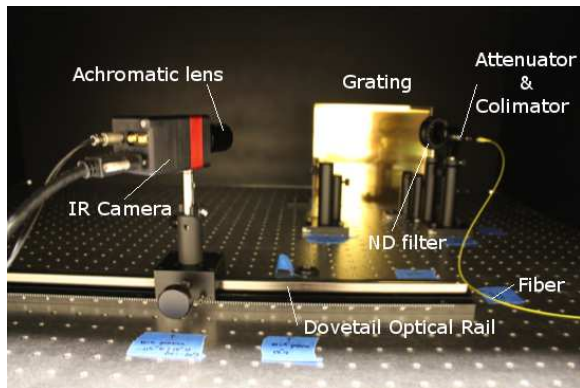


Fig. 8.— A photo of the efficiency measurement configuration in the lab.

the entire experiment to eliminate scattered background light. All the components, except the grating, were kept fixed onto the optical bench until all efficiency measurements were completed. Every time we left the lab, the grating was carefully packed and put away in a secured location.

The collimator focal length and the optical path length were determined by considering the divergence angle of the laser with the goal of keeping the final spot size well inside the detector field of view (FOV). The attenuator and combination of two ND filters are employed to ensure that the final spot on the detector is not saturated at a reasonable exposure time for the brightest order with good signal to noise ratio on the faintest orders. The achromatic camera lens pair is chosen so that only one spot falls on the camera’s detector at a time.

The efficiency is defined as the flux of monochromatic light diffracted into the order being measured relative to the total flux. We measure a pure reflection of the same light source from an un-ruled area on the grating/test ruling (called pure reflection) as the total efficiency. Since the un-ruled part of the grating/test ruling is outside of the clear aperture, and the quality of its surface is not guaranteed, we also use the total sum of all orders (called order sum) as a measure of the total flux as well. Efficiency measurements using both values for total flux are presented in this paper.

A typical efficiency measurement procedure is as follows: 1) set up the grating for the pure reflection;

2) close the bench baffle; 3) find the best exposure time and measure the pure reflection with the laser on; 4) measure the pure reflection with the laser off; 5) open the baffle; 6) set up the grating to place the first order to be measured in the camera’s FOV; 7) close the baffle; 8) find the best exposure time and measure the flux with laser on and off; 9) move the IR camera to the next order; and repeat step 8 and 9 until all orders are measured. In these tests, we measured $m = -13$ to $m = 8$. It takes about one hour to complete this procedure. Since we know that the polarization state of the fiber does not change in one hour (Appendix B) but moving the fiber changes the polarization state of the beam, we were very careful not to touch the fiber during the entire procedure.

The ruled area of the OSIRIS grating is 205×230 mm. To assess the spatial dependence of the efficiency, measurements are made at nine locations (3 by 3 configuration) across the grating surface as illustrated in Figure 9.

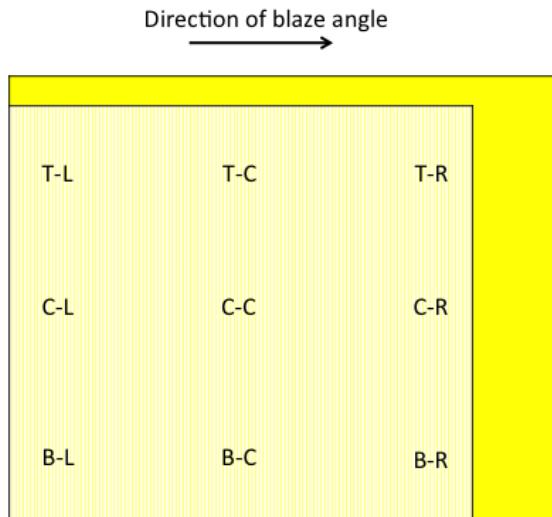


Fig. 9.— Diagram showing the location of the grating efficiency measurements. The light yellow area is the region of the ruled area, 205×230 mm. The bright yellow area is the overall area of the substrate. The arrow indicates the direction of blaze angle.

After the efficiency at one location is measured, we move the grating sideways or change the height of the stage, where the grating sits, to move to the

next location. The grating surface is kept parallel to the dovetail optical rail, and the optical path length is kept the same for all measurement. This allows us to keep the setup fixed as much as possible.

For each grating order, we acquire 100 frames with an additional 100 background frames. The 100 background frames are median combined to make a master background and subtracted from each science frame. Then 100 background subtracted frames are median combined and divided by the exposure time to make the final reduced image. To conserve the optical alignment, we do not take flat frames. A histogram of a normalized flat field taken during testing shows a normal distribution with a standard deviation of 0.024. Instead of applying flat fielding to the final reduced image, we include the flat field fluctuation of 2.4 % as a part of measurement uncertainties.

A two dimensional Gaussian function is fitted to the final reduced image to find the spot center, and the total flux in the spot is obtained by summing up the counts in the biggest circle that can be fit in the final reduced image centered at the spot center. A more detailed discussion of this method is found in Appendix C.

There were two efficiency requirements defined by Keck Observatory and our team which the new grating (G3) had to meet in order to be eligible for installation in OSIRIS:

- (A) Global efficiency requirement: On average, the new grating has to be at least 50 % more efficient than G2, which means >45 % in J -band ($1.310 \mu\text{m}$).
- (B) Field dependent efficiency requirement: The efficiency of the new grating has to be better than G2 efficiency (<30 %) at all location across the grating.

In the next section, we report the results of the new grating efficiency measurements.

3.3. New (G3) and Old (G2) OSIRIS Grating Efficiencies

Before G3 was shipped to the Dunlap Institute for Astronomy & Astrophysics (Dunlap) in July 2012, Bach Research assessed the quality of the wavefront of G3 surface with a 4 inch aperture

Zygo interferometer. Bach Research took wavefront measurements along the center of the grating and moved the aperture from start to the end of the ruling. They performed these measurements across several optical orders to yield an indication of wavefront error over the entire surface. The wavefront quality across the surface is roughly ± 0.5 wave at $\lambda = 632.8 \text{ nm}$.

The peak efficiency ($m = -5$) of G3 with respect to the pure reflection at $\lambda = 1.310 \mu\text{m}$ at nine spatial locations across the grating surface are summarized in Table 3, and Figure 10 shows detailed efficiency for $-13 \leq m \leq 8$. At all nine locations, the peak efficiencies are more than 75 %, and the average efficiency, weighted by error, is 78.0 ± 1.6 % with respect to the pure reflection, and the non-weighted average of 77.8 % with respect to the order sum (see footnotes in Table 3). This grating meets both global and field dependent efficiency requirements stated in §3.2, which led our team to install G3 in OSIRIS in December 2012.

After G3 was installed and its on-sky performance was confirmed through engineering observations, G2 was shipped to Dunlap, and its efficiency was measured using the same setup used for G3.

Table 4 summarizes the peak efficiency at nine locations, and Figure 11 is the result of full efficiency measurements of G2. On average, G2 has a weighted efficiency of 39.5 ± 0.8 % with respect to the pure reflection and 35.8 ± 0.7 % with respect to the order sum.

On average, G3 has a factor of about two greater efficiency at $1310 \mu\text{m}$. We also find that G3 has a close-to-uniform efficiency across the surface compared to G2. The field-dependent standard deviation of G3 peak efficiencies is 2.23 % whereas the field-dependent standard deviation of G2 is 11.68 %.

3.4. Measurement Uncertainties

To estimate the uncertainties in the efficiency measurement, we look at the configuration uncertainty of 1% and flat fielding uncertainty of 2.4 % (§3.2), random camera noise of ~ 10 DN (Appendix A), flux fluctuation due to PCB temperature of 0.3 % (Appendix A) and laser stability of 3.5% (Appendix B). We also estimate the random

TABLE 3
G3 PEAK EFFICIENCY AT 1.310 μm

| Location | Left | Center | Right |
|----------|-------------------|------------------|------------------|
| Top | 82.5 ± 5.1 % | 76.8 ± 4.7 % | 80.4 ± 5.0 % |
| | 78.2 ^a | 77.9 ± 4.2 % | 79.2 ± 4.5 % |
| | 1.05 | 0.99 | 1.01 |
| Center | 76.9 ± 4.8 % | 76.7 ± 4.7 % | 79.3 ± 4.9 % |
| | 76.4 ± 4.3 % | 76.3 ± 4.3 % | 79.4 ± 4.4 % |
| | 1.00 | 1.01 | 1.00 |
| Bottom | 77.6 ± 4.8 % | 75.2 ± 4.6 % | 77.9 ± 4.8 % |
| | 77.6 ± 4.3 % | 76.1 ± 4.1 % | 79.3 ± 4.3 % |
| | 1.00 | 0.99 | 0.98 |

NOTE At each location, there are three values. The first one is the efficiency with respect to the pure reflection, the second one is the efficiency with respect to the order sum, and the last one is the ratio of the order sum to the pure reflection. All values are shown with the associated measurement errors.

^aAfter we reduced all data, one of the original data file ($m = 6$ at TL) was corrupted before we calculated the random observation uncertainty. Thus, the efficiency value is reported here, but not the measurement uncertainty.

TABLE 4
G2 PEAK EFFICIENCY AT 1.310 μm

| Location | Left | Center | Right |
|----------|------------------|------------------|------------------|
| Top | 64.6 ± 4.0 % | 30.6 ± 1.9 % | 31.1 ± 1.9 % |
| | 59.5 ± 3.4 % | 28.7 ± 1.5 % | 29.4 ± 1.5 % |
| | 1.09 | 1.06 | 1.06 |
| Center | 54.8 ± 3.4 % | 50.6 ± 3.1 % | 34.9 ± 2.2 % |
| | 45.3 ± 2.8 % | 41.5 ± 2.6 % | 32.9 ± 1.7 % |
| | 1.21 | 1.22 | 1.06 |
| Bottom | 49.9 ± 3.1 % | 47.0 ± 2.9 % | 37.9 ± 2.3 % |
| | 46.3 ± 2.5 % | 43.4 ± 2.3 % | 35.9 ± 1.8 % |
| | 1.08 | 1.08 | 1.06 |

NOTE At each location, there are three values. The first one is the efficiency with respect to the pure reflection, the second one is the efficiency with respect to the order sum, and the last one is the ratio of the order sum to the pure reflection. All values are shown with the associated measurement errors.

observational error by calculating the pixel-wise standard deviation of the mean using 100 science frames and 100 dark frames per order. The random observational error is very small ($< 0.02\%$) for all cases.

To confirm the repeatability of our measurements and the estimate of the error, we measured G2 efficiency at two locations, top-left and top-center, (see Figure 9 for the location) twice, the second measurement after about two weeks later than the first measurement. The peak efficiency ratio of the first time to the second time is 0.982 (pure reflection) and 0.995 (order sum) for the top-left location, and 1.005 (pure reflection) and 1.011 (order sum) for the top-center location. They are both within the measurement uncertainties.

3.5. Polarization Effect on Grating

The polarization state of the incident light can affect the efficiency of a diffraction grating in many cases. To understand the polarization dependence on the OSIRIS grating efficiency, we modelled the TE (polarized parallel to the groove) and TM (polarized perpendicular to the groove) efficiencies of the OSIRIS grating using RCWA. The RCWA model predicts that the peak TE to TM efficiency ratio for a $1.310\ \mu\text{m}$ monochromatic light source at $m = -5$ is 1.041.

We conducted the polarized efficiency measurement experiments on the test ruling three times using: (1) the IR laser diode (no polarizer); (2) the IR laser diode in TE mode defined by the polarizer; and (3) the IR laser diode in TM mode defined by the polarizer. During the measurement, all the components, especially the fiber was fixed to keep the same polarization state throughout. Figure 12 shows these results where the total efficiency is defined either by the pure reflection (left) or the order sum (right). The peak TE to TM efficiency ratio at $m = -5$ is 1.056 ± 0.092 and 1.029 ± 0.074 for the pure reflection and the order sum, respectively. These measurements are in agreement with the theoretical predictions.

We confirmed that the polarization state of the laser does not change during the full efficiency measurement at one spatial location (§3.2 and Appendix B), and thus individual orders and the pure reflection are measured with the same polarization. As the efficiency is calculated with respect

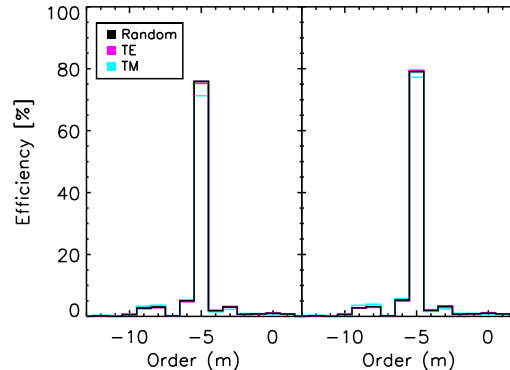


Fig. 12.— Efficiency of the test ruling by Bach Research with respect to the pure reflection (left) and with respect to the order sum (right) measured ($-13 \leq m \leq 2$) using TE/TM modes (magenta/cyan) and no polarizer (black).

to the pure reflection or the order sum, we do not take into account the effect of the polarization in the measurement uncertainty calculation. Between different spatial locations, maximum of 4% difference in efficiency due to TE and TM states can theoretically occur. This polarization effect can also affect the real scientific observation at OSIRIS; however, it is probably insignificant since other noise components, such as sky lines, would be the dominant source of uncertainty.

4. New Grating Installation and Commissioning

OSIRIS was slowly warmed up to ambient temperature over a one week period, and G3 installation was performed in December 2012 by our team. G2 was removed from OSIRIS, and its alignment was measured and marked with respect to the mounting plate in the lab at the Keck Observatory summit facility. G2 was detached from the mounting plate, and G3 was aligned to the marks and installed on the mounting plate.

Figure 13 shows a HeNe laser at $632.8\ \text{nm}$ being diffracted by G2 (top) and G3 (bottom) in the Keck summit lab prior to the installation of G3 in OSIRIS. The light is visibly more concentrated to one order for G3 while a higher fraction of light is diffracted to multiple orders by G2.

On January 20 and 27, 2013, OSIRIS with G3



Fig. 13.— Diffraction of a HeNe laser at 632.8 nm using G2 (top) and G3 (bottom). Test performed in December 2012. The light is more concentrated in one order for G3 whereas high fraction of light is diffracted in multiple orders for G2.

was commissioned on-sky using the Keck-I AO system. Both nights started with clear night, but unfortunately, within one or two hours, the weather conditions changed to thin/high cirrus with high wind. Some standard stars and blank sky were observed with the deformable mirror off. The resulting measurements are certainly affected by the varying weather conditions. The measurements of OSIRIS sensitivity with G3 in each spectrograph filter from these nights, as well as prior measurements with G2 are reported in §5.

5. On Sky Performance and Throughput

In this section, we compare on-sky performance between G2 and G3. Our comparison is complicated by the fact that in early 2012 OSIRIS was moved from Keck-II to Keck-I to be the first dedicated science instrument for a new Laser Guide Star (LGS) AO capability on Keck-I that was installed in 2010. The LGS system on Keck-I uses a significantly improved laser system compared to the existing Keck-II laser system (Chin et al. 2010).

The final zero point magnitude at all broadband filters for OSIRIS are calculated using standard star observations. The data used to calculate G2 zero points were all taken on Keck-II, and G3 data were all taken on Keck-I. Although there are dif-

ferences in throughput between the two telescopes and AO systems as well as differing weather condition between our limited observations, there is a general zero point improvement for G3 in comparison to G2.

We use as many standard star observations as we had access to, but the number of observations is fairly small in each particular band. For OSIRIS with G2 on Keck-II, HD105601, HD106965, HD201941, and HD18881 taken between April 2007 and January 2012 are used, and for OSIRIS with G3 on Keck-I, HD44612 and HD18881 observed on January 20 and 27, 2013 are used. The zero points are calculated by applying a large rectangular aperture on raw (non-reduced) image, over the entire spectrum. In all cases, approximately equal rectangles are used for the wavelength ranges. The resulting zero point magnitude and the factors of improvement are shown in Table 5.

6. Conclusion

OSIRIS at W. M. Keck Observatory is a particularly unique IFS instrument among other IFSs with AO capability today in use of a single fixed exceptionally coarse ruling (27.93 grooves per mm) diffraction grating, which uses $m = -3, -4, -5$, and -6 to cover K, H, J , and Z bands. While OSIRIS has delivered a number of important scientific results, its sensitivity was limited by the performance of its spectrograph grating. Our team has worked with a new grating vendor, Bach Research Corporation, to produce a better quality grating for OSIRIS.

Bach Research manufactured a test ruling and the new grating (G3) in 2012, and we have carefully measured the direct efficiencies of both at $1.310 \mu\text{m}$ in the lab. The weighted field-averaged peak efficiency of G3 is $78.0 \pm 1.6 \%$ (pure reflection) and 77.8% (order sum) (see footnotes in Table 3) with a field standard deviation 2.23% (pure reflection) and 1.32% (order sum). After the G3 efficiency was confirmed to be high and close to uniform over the surface, G3 was installed to OSIRIS in December 2012. G2 was shipped to Dunlap after G3 performance was tested and confirmed on-sky in January 2013. G2 efficiency was as well measured using the same lab setup used for the G3 measurement. For G2, the weighted field-

TABLE 5
ZERO POINT VEGA MAGNITUDE AND FACTOR OF IMPROVEMENT FROM G2 TO G3

| Filter λ_{cen} [μm] | <i>Zbb</i> | <i>Jbb</i> | <i>Hbb</i> | <i>Kcb</i> | <i>Kbb</i> |
|---|------------|------------|------------|------------|------------|
| G2 at Keck-II | 23.70 | 23.80 | 24.45 | 23.19 | 23.67 |
| G3 at Keck-I | 24.19 | 24.22 | 24.84 | 24.16 | 24.54 |
| Improvement | 1.56 | 1.48 | 1.43 | 2.45 | 2.23 |

averaged peak efficiency is 39.5 ± 0.8 % (pure reflection) and 35.8 ± 0.7 % (order sum) with a field standard deviation is 11.68 % (pure reflection) and 9.82 % (order sum).

The new OSIRIS grating gives a factor of about two times increase in average efficiency at 1.310 μm with less field-dependent efficiency change across the surface. The final sensitivity improvement was difficult to assess because OSIRIS was moved from Keck-II to Keck-I in early 2012; however, we were able to determine the zero point magnitudes and factors of improvement for each broadband filter. On average, on-sky throughput is 1.83 times better than when it was at Keck-II with G2. This enables us to observe fainter objects and to use observing time more efficiently.

A single fixed diffraction grating with a coarse ruling can reach high efficiency and perform well on OSIRIS, but it is very difficult to engineer, and only a few companies exist worldwide who can manufacture such a grating today. For the next generations of IFS instrumentation, the more usual approach of using finer ruling grating with $m = 1$ order may be better suited. For example, IRIS on TMT, an IFS with some characteristics and design elements similar to OSIRIS, will instead have several gratings with finer groove densities of ~ 150 to 900 per mm (Moore et al. 2010; Larkin et al. 2010).

Acknowledgements

We particularly want to thank the Bach Research Corporation for all of their efforts and support during the selection and fabrication of the OSIRIS grating. We enjoyed working with the Bach Research Corp. team during this entire process. We also thank the Keck Observatory

staff who helped with the planning and installation work for the new grating in OSIRIS. The new OSIRIS grating was graciously funded by the Dunlap Institute for Astronomy & Astrophysics at University of Toronto. Funding for this project was also provided by the NSERC Discovery grant (RGPIN 419376) and the Canada Foundation for Innovation grant (31773). Our on-sky data presented herein were obtained at the W.M. Keck Observatory, which is operated as a scientific partnership among the California Institute of Technology, the University of California, and the National Aeronautics and Space Administration. The Observatory was made possible by the generous financial support of the W.M. Keck Foundation. The authors wish to recognize and acknowledge the very significant cultural role and reverence that the summit of Mauna Kea has always had within the indigenous Hawaiian community. We are most fortunate to have the opportunity to conduct observations from this mountain.

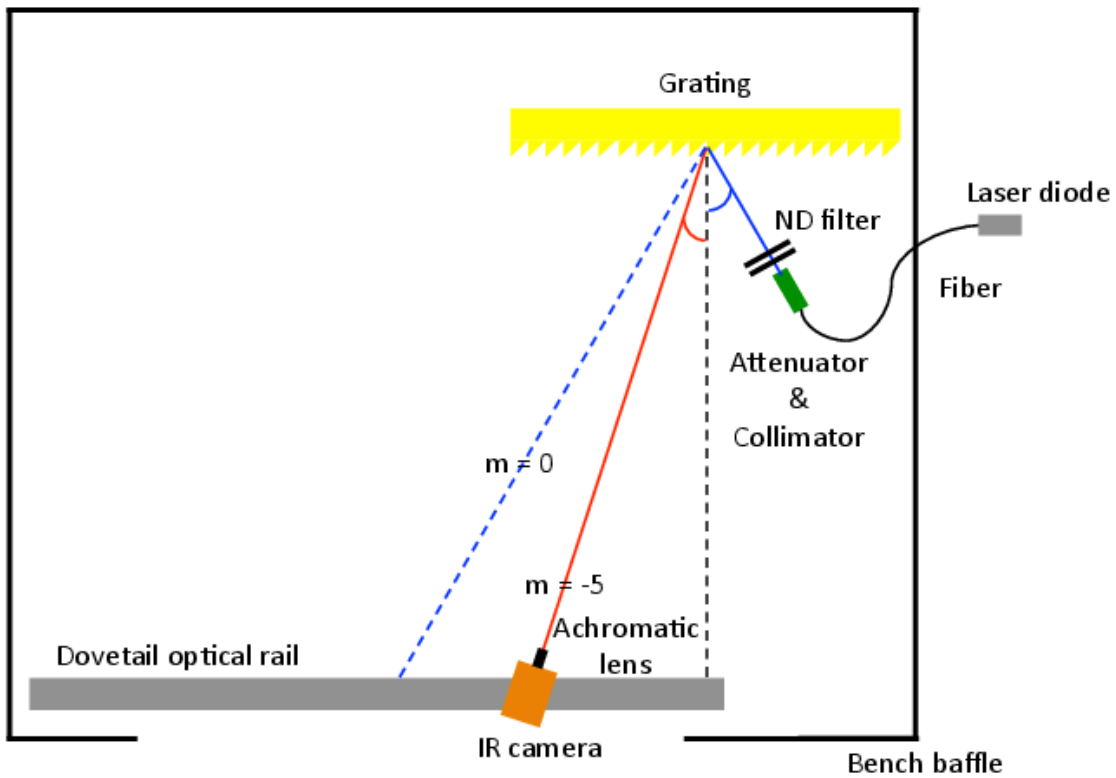


Fig. 7.— Schematic of the efficiency measurement configuration in the lab (not to scale). The entire setting is covered up by an aluminum baffle box to control background and scattered light.

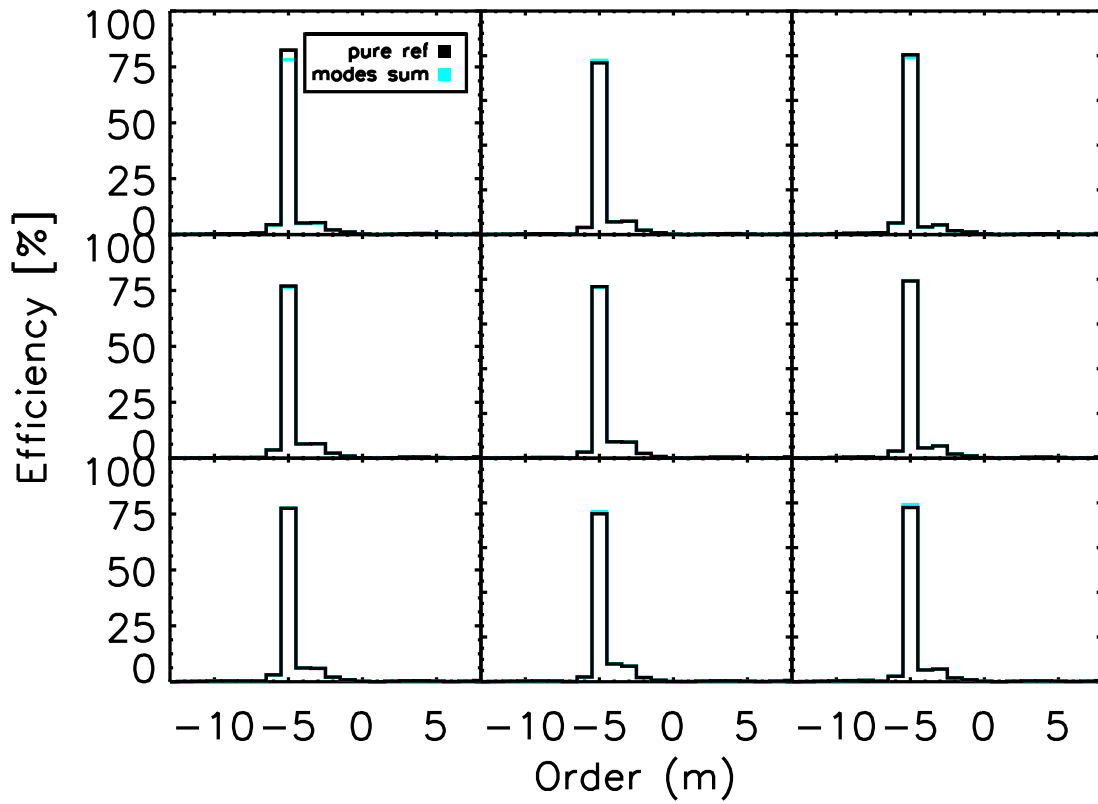


Fig. 10.— Efficiency of G3 by Bach Research with respect to the pure reflection (black) and with respect to the order sum (cyan) measured at $-13 \leq m \leq 8$.

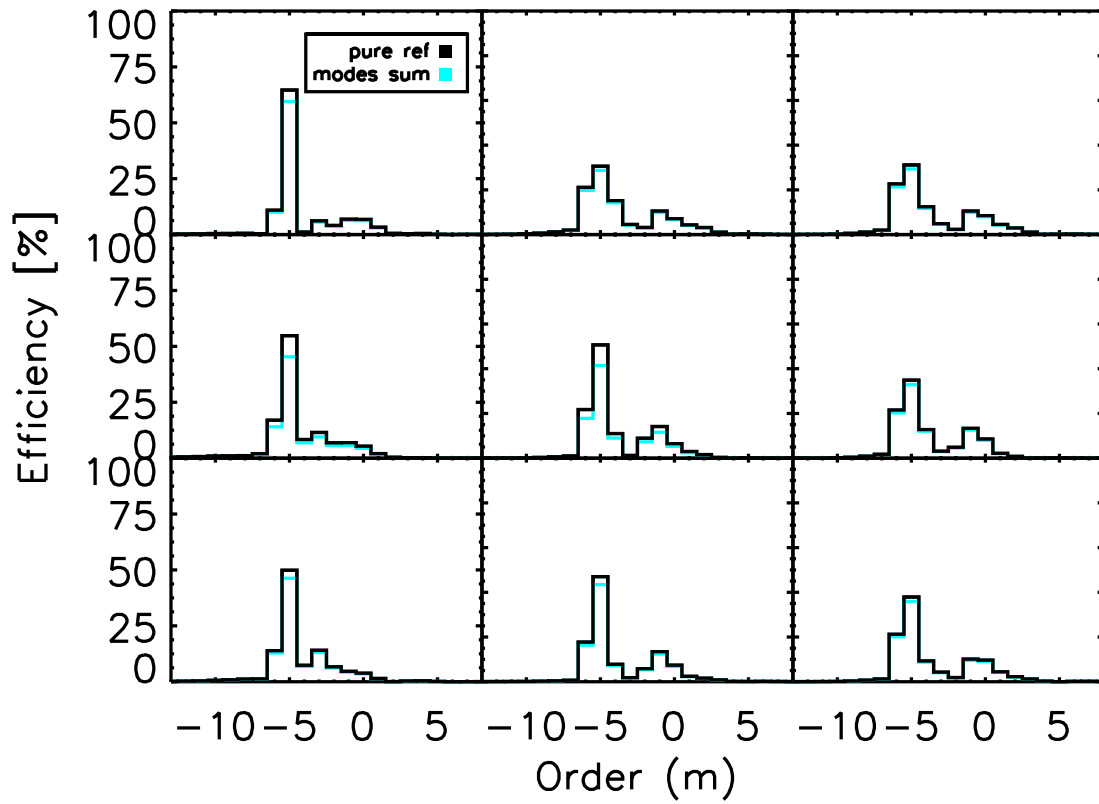


Fig. 11.— Efficiency of G2 by Diffraction Products with respect to the pure reflection (black) and with respect to the order sum (cyan) measured at $-13 \leq m \leq 8$.

A. Camera Linearity

We evaluated the linearity of the InGaAs camera, Raptor Photonics OWL SW 1.7 CL-320, by measuring the average dark counts on the detector as a function of exposure time. The 100 dark frames per grating order taken at the time of efficiency measurements were median combined to make the master dark, and the average of the master dark was plotted as a function of exposure time on Figure 14. All camera settings were

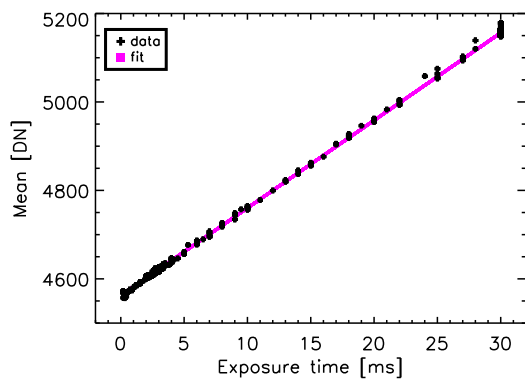


Fig. 14.— Average dark counts vs. exposure time at the time of efficiency measurements. The data were fit by a straight line shown over plotted in magenta.

kept fixed for all times except for the exposure time. Figure 15 shows the absolute difference between data points and the straight line fit, with the Poisson noise over plotted in cyan. The result shows that regardless of the exposure time, there are about 10 DN fluctuations until the Poisson noise takes over at around $t_{exp} = 10$ ms. Hence, we include 10 DN in the noise calculation.

We also looked at the effect of the camera temperature over an hour, which is the amount of time taken for an efficiency measurement of a single spatial position on the grating surface over a large range of orders. In this test, we took images of the laser spot at $t_{exp} = 0.2$ ms every 60 seconds for one hour and repeated the process twice. During the test, the camera and the laser were kept on all the time. The laser was imaged to include the effect of the laser heating up the image sensor in case that happened. Figure 16 shows the changes of two different camera temperatures over one hour

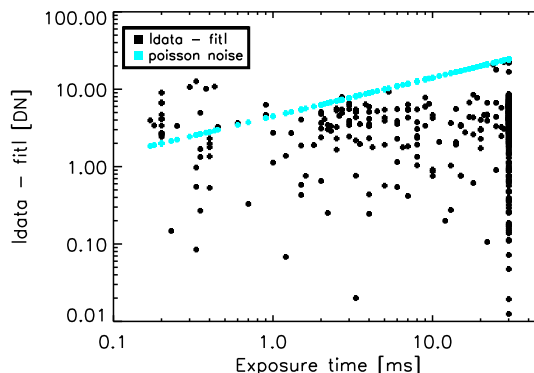


Fig. 15.— Absolute difference between the average dark count and the linear fit plotted as a function of exposure time, with the Poisson noise overplotted in cyan.

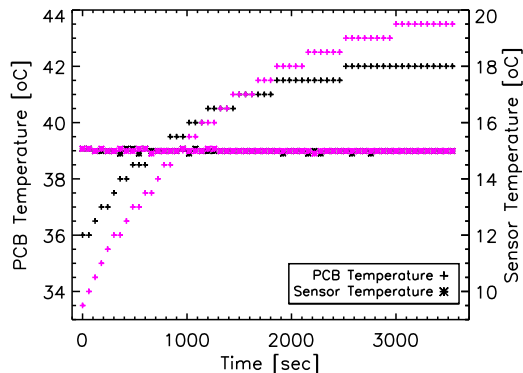


Fig. 16.— Sensor and PCB temperature changes over one hour. With the TEC temperature set to 15 °C, the sensor temperature stayed almost constant while the PCB temperature increased 5 to 10°C. The magenta points are the measurements from the first test, and the black points are the measurements from the second test.

period. Our input temperature (TEC temperature) was always 15°C, and the sensor temperature was almost always constant around 15°C, but the printed circuit board (PCB) temperature increased about 10°C during the first test and about 6°C during the second test over a one hour period.

The distribution of PCB temperatures and the distribution of exposure times used during G2 and G3 efficiency measurements combined is shown in

Figure 17, and Figure 18. Samples taken at t_{exp}

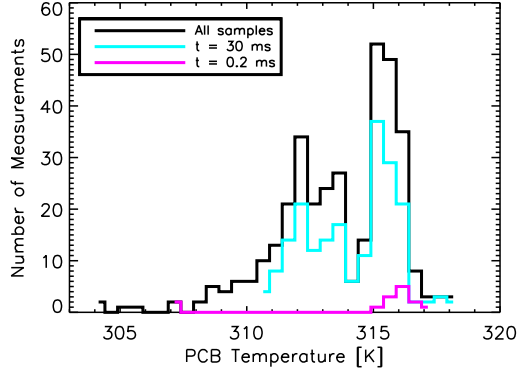


Fig. 17.— The distribution of PCB temperature during G2 and G3 efficiency measurements combined. Black line is the distribution among all samples whereas cyan and magenta are among $t = 30$ ms and $t = 0.2$ ms respectively.

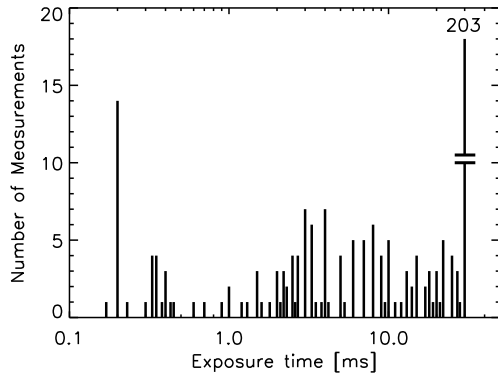


Fig. 18.— The distribution of measurements in an exposure time space during G2 and G3 efficiency measurements combined.

$t = 30$ ms are dominant because G3 and G2 efficiency measurements were all taken with a frame rate of 25 Hz, and taking into account the trigger delay and data transfer, we set the maximum exposure time to be $t_{max} = 30$ ms. The exposure times for individual measurements were chosen to maximize signal level while maintaining the exposure below the saturation, but since we set a maximum exposure time threshold, many fainter spot images were taken with the maximum exposure

time.

Figure 19 shows average dark counts, normalized by the average of all the average dark counts, as a function of the PCB temperature change. The

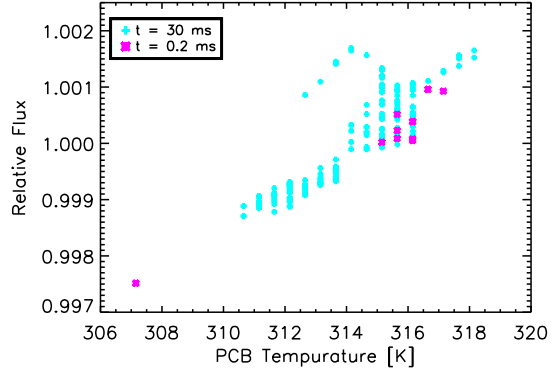


Fig. 19.— The relative flux change of $t = 30$ ms (cyan) and $t = 0.2$ ms (magenta) average dark counts due to the PCB temperature change.

flux increases about 0.6 % as the PCB temperature increases about 10°C . We do not have the information on how long the camera was turned on during the experiments, but we know that to measure the full efficiency at one location, it takes about one hour, and in one hour the PCB temperature changes about 10°C (Figure 16). Combined this information and Figure 19, we take 0.3 % (a half of the full increase in flux) as noise due to camera PCB temperature changes during the efficiency measurements.

B. Infrared Laser Diode Stability Test

We used a $1.310 \mu\text{m}$ laser diode coupled to a SMF-28 fiber as a light source for infrared measurement. To ensure consistency in our measurements, we measured the stability of the laser by monitoring its intensity using the infrared camera tested in Appendix A. First, we fixed the exposure time to $t_{exp} = 0.2$ ms and took a series of images separated by three time intervals: 5, 20, and 60 seconds (Figure 20). The camera and the laser were kept being on until all measurements in a particular sequence were completed. These measurements allowed us to search for any time dependent instabilities in the combined system of

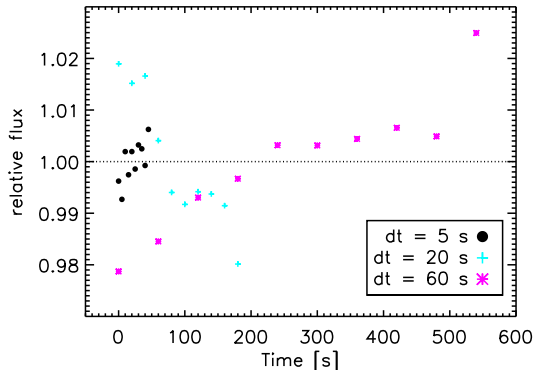


Fig. 20.— Relative flux of the 1.310 μm laser diode versus time for three time intervals: 5 (black circle), 20 (cyan cross), and 60 (magenta star) seconds.

laser and camera. We found the fluctuation in the system seems independent of the time interval of data taken but dependent on the duration of the laser is on.

The polarization of stimulated emission is parallel to the diode junction plane, and thus laser diodes are usually linearly polarized. When a laser is used in a polarization dependent setup, intensity fluctuations can occur due to changing polarization states. Our laser diode is coupled to a SMF-28-J9 step-index fiber with a numerical aperture (NA) of 0.14 and an 8.2 μm diameter core. For this fiber, the dimensionless normalized frequency or normalized thickness of the guide (V) is,

$$V = kd(NA), \quad (\text{B1})$$

where k is the wave number, and d is the fiber core radius (e.g. Iizuka 2002) of 2.75 at 1310 μm . The first critical frequency (cutoff V) for single mode operation is 2.405, and therefore our fiber supports four polarization modes. To understand the polarization characteristics of our laser, we tested the laser stability with and without a calcite polarizer in the optical path. We took a series of images of laser beam for an hour at 60 s intervals. We performed these measurements twice: once with a calcite polarizer in front of the laser and once without the polarizer. The polarizer was oriented so that the output beam had the maximum intensity (direction of the polarization of the laser is parallel to the direction of polarizer). After one hour

of measurement, we verified that the peak intensity from the polarizer was still at the same angle. This means, over one hour, the polarization state of the laser did not change, and therefore we assume the laser polarization state does not change during the efficiency measurements.

Figure 21 shows that the laser flux fluctuates 3.5 % (one-half of (highest - lowest) flux) over one hour. The initial discrepancy up to 1000 s between

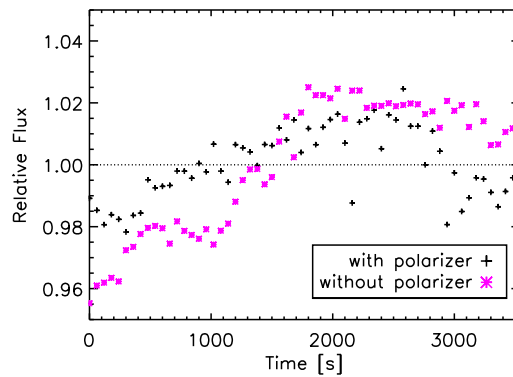


Fig. 21.— Relative flux of the 1.310 μm laser diode versus time for a 60 second interval with a polarizer (black) and without a polarizer (magenta).

the measurements with and without the polarizer is probably due to room/detector temperature differences because the two measurements were taken on different days. Since the polarization state of the laser did not change over one hour, this variation is probably from the laser itself as shown in Figure 20. We take into account this 3.5 % laser flux variation in the noise calculation.

C. Total Flux in a Spot

The grating efficiency is measured by summing up the flux in an individual spot at a particular order and dividing by the total flux. To confirm that we collect all flux in an individual spot, we tested two methods. One is by Gaussian fitting. A two dimensional Gaussian function is fitted to the final reduced image, and aperture photometry is applied to both the reduced image and the 2D Gaussian function. Figure 22 shows the growth curves of the reduced image (black) and the Gaussian (magenta) for the test ruling. They are both

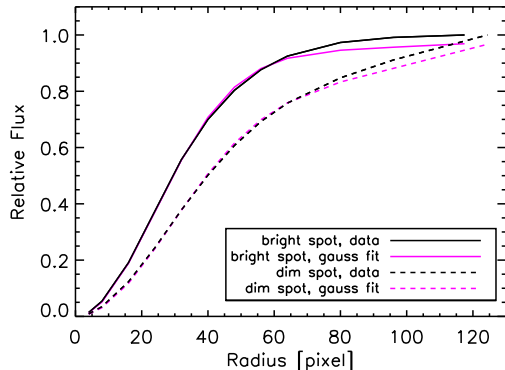


Fig. 22.— Growth curves of the reduced image (black) and 2D Gaussian fit (magenta) for the test ruling. The solid lines are for the brightest spot, and the dashed lines are for a dim spot whose optical path is the longest whose size is therefore the biggest on the detector.

normalized to the reduced image total flux. The solid line is the growth curve of the brightest spot, and the dashed line is of a dimmer spot. The optical path of the dimmer spot is the longest and thus the spot size is biggest on the detector due to the divergence angle of the laser beam. The maximum radius on the plot is the radius of a biggest circle that can be fitted in the frame centered at the Gaussian fit center. For both bright and dim spots, two lines are quit similar. Figure 23 shows the efficiency of the test ruling with respect to the pure reflection, using the aperture photometry of the reduced image (black) and the integrated sum of the Gaussian to infinity (magenta). Two plots are almost exactly the same.

The growth curve and efficiency comparisons illustrate that our experiment and optical setup is optimized with respect to the laser spot size at the detector and the detector plate scale. Since two cases give similar answers, we deploy the simple aperture photometry method to the reduced image to calculate the total counts in a spot.

D. Pipeline Modification

One unique aspect of OSIRIS is that over 3000 spectra are all partially overlapped on the detector at staggered wavelength, and hence special re-

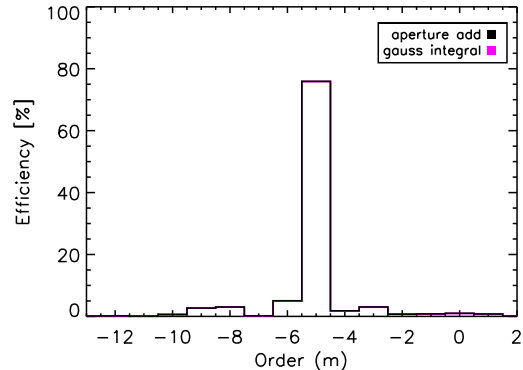


Fig. 23.— Efficiency of the test ruling with respect to the pure reflection. For the two cases, a circular aperture applied to the reduced image (black) and Gaussian fit integral (magenta), the efficiencies are almost on top of each other.

duction and calibration steps are required. The OSIRIS Data Reduction Pipeline (DRP) reduces the science data to the level where a user can begin their custom scientific analysis. After OSIRIS was moved to Keck-I, and G3 was installed, the DRP had to be modified to account for the new AO system and the new grating.

On Keck-I, the AO system optical path to OSIRIS has one less mirror than the Keck-II system. This produces a flipping of image in the y-direction. This axis flip is fixed in the DPR “Assemble Data Cubes” module. The Keck-I AO system uses a different IR/visible splitting dichroic from that used on Keck-II, and white light measurements using the AO fiber calibration source showed that the Keck-I AO system dichroic produces essentially no instrumental dispersion. The “Correct Dispersion” module in the DRP that corrects for atmospheric dispersion and instrumental dispersion was appropriately modified for the Keck-I AO path.

We determined a new wavelength solution using arc lamp and OH lines in each broadband filter, and we found about four spectral channels of shift from the previous (G2) version. The field dependent wavelength solution per spaxel was calculated using the cross correlation of OH lines using the Kn3 filter with the 35 mas spaxel scale. Figure 24 shows relative/absolute pixel and angstrom wave-

length offsets between 2006 with G2 (top) and 2013 with G3 (bottom). It is a residual offsets after using the “Assemble Data Cubes” and a new wavelength solution. The comparison of two confirms that the quality of the ruling on the new grating is more uniform across the surface. The field dependent and global wavelength solution is now implemented in the new pipeline.

A problem had been observed prior to commissioning of G3 that affected the lower right quadrant of the reduced data cube with varying shifts in measured intensity and shifts in the detector channel offsets. During the modification of the DRP, we found that there appeared to be a bad column on the detector, and this was biasing the wavelength solution. This problem started on September 17, 2011 when one of the spectrograph Hawaii-II detector Leach-ARC detector read-out video boards was swapped. In the end, it is just one pixel shift that skews the timing of the entire channel. This channel offset is now fixed in the new pipeline within the “Subtract Frame” module.

All these modifications are implemented in the new version of the DRP, and the DRP full package is now available to download at the OSIRIS instrument webpage².

REFERENCES

- Barman, T. S., Macintosh, B., Konopacky, Q. M., & Marois, C. 2011, *ApJ*, 733, 65
- Chin, J. C. Y., Stalcup, T., Wizinowich, P., et al. 2010, in *Society of Photo-Optical Instrumentation Engineers (SPIE) Conference Series*, Vol. 7736, *Society of Photo-Optical Instrumentation Engineers (SPIE) Conference Series*
- Contini, T., Garilli, B., Le Fèvre, O., et al. 2012, *A&A*, 539, A91
- Davies, R. I., Müller Sánchez, F., Genzel, R., et al. 2007, *ApJ*, 671, 1388
- Do, T., Ghez, A. M., Morris, M. R., et al. 2009, *ApJ*, 703, 1323
- Do, T., Lu, J. R., Ghez, A. M., et al. 2013, *ApJ*, 764, 154
- Förster Schreiber, N. M., Genzel, R., Lehnert, M. D., et al. 2006, *ApJ*, 645, 1062
- Iizuka, K. 2002, *Elements of Photonics*, Vol. 2 (New York: A John Wiley & Sons, Inc.)
- Konopacky, Q. M., Barman, T. S., Macintosh, B. A., & Marois, C. 2013, *Science*, 339, 1398
- Larkin, J., Barczys, M., Krabbe, A., et al. 2006, in *Society of Photo-Optical Instrumentation Engineers (SPIE) Conference Series*, Vol. 6269, *Society of Photo-Optical Instrumentation Engineers (SPIE) Conference Series*
- Larkin, J. E., Quirrenbach, A., Krabbe, A., et al. 2003, in *Society of Photo-Optical Instrumentation Engineers (SPIE) Conference Series*, Vol. 4841, *Society of Photo-Optical Instrumentation Engineers (SPIE) Conference Series*, ed. M. Iye & A. F. M. Moorwood, 1600–1610
- Larkin, J. E., Moore, A. M., Barton, E. J., et al. 2010, in *Society of Photo-Optical Instrumentation Engineers (SPIE) Conference Series*, Vol. 7735, *Society of Photo-Optical Instrumentation Engineers (SPIE) Conference Series*
- Laver, C., & de Pater, I. 2009, *Icarus*, 201, 172
- Law, D. R., Steidel, C. C., Erb, D. K., et al. 2009, *ApJ*, 697, 2057
- Lyke, J. E., & Campbell, R. D. 2009, *AJ*, 138, 1090
- McConnell, N. J., Ma, C.-P., Gebhardt, K., et al. 2011, *Nature*, 480, 215
- McGregor, P. J., Bloxham, G. J., Boz, R., et al. 2012, in *Society of Photo-Optical Instrumentation Engineers (SPIE) Conference Series*, Vol. 8446, *Society of Photo-Optical Instrumentation Engineers (SPIE) Conference Series*
- Moharam, M. G., & Gaylord, T. K. 1981, *Journal of the Optical Society of America (1917-1983)*, 71, 811
- Moore, A. M., Bauman, B. J., Barton, E. J., et al. 2010, in *Society of Photo-Optical Instrumentation Engineers (SPIE) Conference Series*, Vol. 7735, *Society of Photo-Optical Instrumentation Engineers (SPIE) Conference Series*

²<http://www2.keck.hawaii.edu/inst/osiris/>

- Thatte, N. 2010, *The Messenger*, 140, 26
- Trippe, S., Gillessen, S., Gerhard, O. E., et al. 2008, *A&A*, 492, 419
- Wisnioski, E., Glazebrook, K., Blake, C., et al. 2011, *MNRAS*, 417, 2601
- Wizinowich, P. L., Le Mignant, D., Bouchez, A. H., et al. 2006, *PASP*, 118, 297
- Wright, S. A., Larkin, J. E., Law, D. R., et al. 2009, *ApJ*, 699, 421

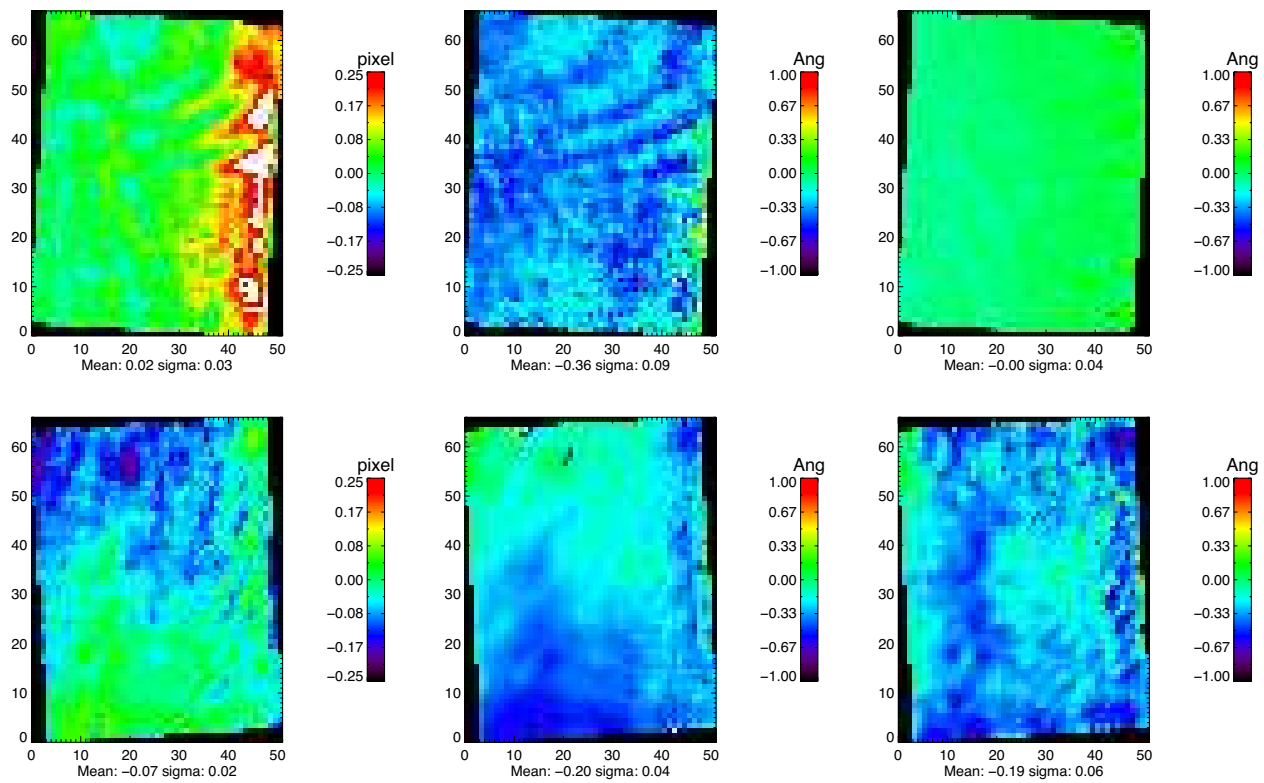


Fig. 24.— Uncorrected relative pixel shift (left), uncorrected absolute angstrom offsets (middle), and corrected absolute angstrom shift (right) for Kn3 35 mas in 2006 with G2 (top) and in 2013 with G3 (bottom).